J Neurophysiol 96: 3237–3247, 2006.
First published September 13, 2006; doi:10.1152/jn.00488.2006.

Large-Scale Organization of Preferred Directions in the Motor Cortex. II. Analysis of Local Distributions

Thomas Naselaris,[1] Hugo Merchant,[1,2,6] Bagrat Amirikian,[1,2] and Apostolos P. Georgopoulos[1,2,3,4,5]

[1]*Brain Sciences Center, Veterans Affairs Medical Center;* [2]*Department of Neuroscience,* [3]*Department of Neurology, and* [4]*Department of Psychiatry, University of Minnesota Medical School;* [5]*Cognitive Sciences Center, University of Minnesota, Minneapolis, Minnesota; and* [6]*Instituto de Neurobiología, Universidad Nacional Autónoma de México, Campus Juriquilla, Querétaro, Mexico*

Submitted 8 May 2006; accepted in final form 6 September 2006

Naselaris, Thomas, Hugo Merchant, Bagrat Amirikian, and Apostolos P. Georgopoulos. Large-scale organization of preferred directions in the motor cortex. II. Analysis of local distributions. *J Neurophysiol* 96: 3237–3247, 2006. First published September 13, 2006; doi:10.1152/jn.00488.2006. The spatial arrangement of preferred directions (PDs) in the primary motor cortex has revealed evidence for columnar organization and short-range order. We investigated the large-scale properties of this arrangement. We recorded neural activity at sites on a grid covering a large region of the arm area of the motor cortex while monkeys performed a 3D reaching task. Sites were projected to the cortical surface along anatomically defined cortical columns and a PD was extracted from each site with directionally tuned activity. We analyzed the resulting 2D surface map of PDs. Consistent with previous studies, we found that any particular reaching direction was rerepresented at many points across the recorded area. In particular, we determined that the median radius of a cortical region required to represent the full complement of reaching directions is at most 1 mm. We also found that for the majority of regions of this size, the distribution of PDs within them exhibits an enrichment for the representation of forward and backward reaching directions (see companion paper). Finally, we found that the error of a population vector estimate of reaching direction constructed from neural activity within these regions is small on average, but varies significantly across different sections of the motor cortex, with the highest levels of error sustained near the fundus of the central sulcus and lowest levels achieved near the crown. We interpret these findings in the context of two well-known features of motor cortex, that is, its highly distributed anatomical organization and its behaviorally dependent plasticity.

INTRODUCTION

The spatial organization of the primary motor cortex (M1) has been analyzed chiefly in the context of its representation of muscles, joints, and body parts (Andersen et al. 1975; Asanuma and Rosen 1972; Cheney and Fetz 1985; Cheney et al. 1985; Donoghue et al. 1992; Fetz and Cheney 1978, 1980; Fischl et al. 1999; Gould et al. 1986; Humphrey and Reed 1983; Huntley and Jones 1991; Kwan et al. 1978; Park et al. 2001; Penfield and Boldrey 1937; Penfield and Rasmussen 1950; Schieber and Hibbard 1993; Strick and Preston 1978; Waters et al. 1990). Throughout several decades of mapping studies, experimenters have used a variety of techniques for electrically activating regions of the motor cortex and then attempted to relate the sites of activation with evoked muscle contractions or movements of body parts about specific joints. However, this historical emphasis on mapping somatotopic representations in the motor cortex belies the fact that M1 is not simply a map of the body's musculature. M1 maintains a representation of higher-order features of movement, most notably the direction of reaching (Caminiti et al. 1991; Georgopoulos et al. 1982, 1984, 1986; Schwartz 1994). A large percentage of cells in the arm region of the motor cortex generate patterns of discharge that vary systematically with respect to the reaching direction of the arm (Schwartz et al. 1988). Given the precedent set by years of research on the somatotopic organization of M1, it is natural to ask how the spatial organization of M1's directional representation is structured.

A cell's representation of reaching direction is characterized by its preferred direction (PD), which is the direction of reach at which the cell's discharge rate peaks (Georgopoulos et al. 1982, 1986; Schwartz et al. 1988). We investigated the spatial organization of direction representation by extracting PDs from activity at recording sites on a grid covering the arm area of M1 of two rhesus macaques engaged in a three-dimensional (3D) center-out task (Georgopoulos et al. 1986).

Previous research on this topic has focused on the spatial organization of PDs over small ($<$1 mm) distances (Amirikian and Georgopoulos 2003; Ben-Shaul et al. 2003; Georgopoulos et al. 1984). These studies analyzed PD differences as a function of the displacement of recording sites along single electrodes and revealed evidence for short-range correlations and columnar organization. However, the data used in those studies did not allow for direct observation of the layout of PDs across the tangential dimension of the cortex (parallel to the cortical surface). The goal of the current study was to assemble a surface map of PDs that would reveal this layout and to analyze this map for large-scale patterns or trends.

Using methods detailed in the companion paper and in Naselaris et al. (2005), we constructed, for each monkey, a surface map of PDs that extended from near the fundus of the central sulcus to the exposed part of the precentral gyrus. To our knowledge, these maps are the first depiction of the surface layout of the 3D PDs in the motor cortex. Of the many ways in which such maps could be analyzed, we focus our analysis in this paper on questions raised by the companion paper. As such, our emphasis in this work will be to describe the distribution of PDs within local regions of the map and to characterize the effect that these distributions have on the

Address for reprint requests and other correspondence: A. Georgopoulos, Brain Sciences Center, Veterans Affairs Medical Center, University of Minnesota, Minneapolis, MN 55455 (E-mail: omega@umn.edu).

The costs of publication of this article were defrayed in part by the payment of page charges. The article must therefore be hereby marked "*advertisement*" in accordance with 18 U.S.C. Section 1734 solely to indicate this fact.

decoding of reaching direction from local populations. Questions regarding the possibility of orderly variation of PDs within such regions will be the topic of a separate work.

In the companion paper, we demonstrated that the distribution of PDs extracted from cells dispersed across the motor cortex has a characteristic structure defined by two salient properties: *1*) a broad distribution of PDs across the directional continuum and *2*) an enrichment for forward and backward reaching directions. These findings raised an important question: Are these features of the global distribution replicated locally or do each of the properties of the global distribution derive from spatially segregated cortical domains? To answer this question, we partitioned the map into local, overlapping subregions, and analyzed the distribution of PDs within each region. We found that the distribution of PDs within local regions of size at most 3 mm^2 replicate the salient features of the global distribution, exhibiting a broad representation of the full 3D continuum of reaching directions, and an enrichment of the representation for forward and backward reaching directions. We also used the neuronal population vector (NPV) to measure error in decoding the direction of reach from neural populations within local regions. We found that these errors are quite small on average, but vary significantly as the result of changes in the breadth of the local distribution. Thus M1 appears to be organized into localized territories, each of which contains a representation sufficient to determine the direction of reach, many of which favor reaches in the forward direction. We argue that these results are consistent with the highly divergent nature of motor-cortical projections to motoneuronal pools (Georgopoulos 1988, 1996) and with the capacity of motor-cortical circuits for behaviorally dependent reorganization. We also discuss the implications of these results for neuroprosthetic design using motor-cortical signals.

METHODS

Behavioral task

All neural data used in these studies were collected from two monkeys (monkeys A and B from companion paper) performing a 3D center-out reaching task. Details are provided in the companion paper and in previous publications (Georgopoulos et al. 1986; Schwartz et al. 1988).

Mapping procedure

All recordings were obtained from the arm region of the M1. The recorded area was contained within a region that extended 3–4 mm along the central sulcus and 7–12 mm in the direction perpendicular to the central sulcus. This region was centered nearly 15 mm from the midline along the medial–lateral axis. Microstimulation (3-ms biphasic pulses for 30 ms at 5–20 μA) within the boundaries of this region evoked contractions of proximal and/or distal arm muscles.

The techniques used to construct a map of recording sites were previously described in detail elsewhere (Naselaris et al. 2005). Briefly, an array of 16 electrodes was passed through the arm region of M1 while monkeys engaged in the reaching task. Before insertion, electrodes were coated in a fluorescent dye. Once the top of neural activity was identified, electrodes were advanced at 150-μm increments until they reached white matter. Raw extracellular potentials were recorded at each site with a sampling frequency of 60 kHz and high-pass filtered at 0.5 kHz.

After the experiment, the monkey was killed and the recorded area of the cortex was blocked and sectioned every 50 μm. Registered digital fluorescence and Nissl-stained images of each slice were used to reconstruct the trajectories made by the electrodes passing through the cortex.

Electrode penetrations passed from the exposed surface of the precentral gyrus, through the crown, and into the anterior bank of the central sulcus (CS). Recording sites were transformed into a "flattened" coordinate system that had the effect of unfolding the cortical surface about the crown of the CS. In all of the maps to be presented, the top/bottom borders of the map are orthogonal to the CS, with the fundus of the CS located on the far left. The left/right borders of the maps are parallel to the CS, with the most medial positions at the top of the maps. In these surface maps, recording sites are projected to the surface along the line defined by neighboring anatomical columns, as revealed by inspection of Nissl-stained sections.

Neural recordings and calculation of PDs

The raw extracellular potentials recorded at each site were converted into multiunit activity (MUA) by applying a 40- to 70-μV amplitude threshold. The exact threshold was determined manually and separately for each recording site. At each recording site, MUA was used to calculate a single PD, using the same multiple linear regression analysis (Georgopoulos et al. 1986) described in the companion paper. Cells were included in the database on the basis of a bootstrap test for significance of directional tuning (Lurito et al. 1991). Because the directional tuning of motor-cortical cells is a well-replicated and robust finding, we used a one-tailed significance criterion ($P < 0.1$).

PDs extracted from MUA were used in all of the analyses presented here. To validate the use of MUA, we selected a subset of our recording sites (data presented in the preceding paper for monkeys A and B) and used Plexon software (Plexon, Dallas, TX) to obtain single-unit activity (SUA). Each site yielded an average of roughly two distinguishable cells. A comparison of PDs extracted from SUA of cells at one site to those extracted from MUA at the same site showed a negligible difference (median angular deviation was 18°, which is within the margin of error for estimating a cell's PD; comparison was based on 848 SUA PDs extracted from 524 sites).

Analyses of the spherical distribution of PDs

SPHERICAL COORDINATES. A PD is a unit vector and may be considered as a point on the surface of a sphere with its center at the starting position for the reaching movements. In this consideration, a PD is specified by a pair of polar angular components (θ, ϕ). $\theta\epsilon$ [0, 180] gives the angular deviation of the PD from the north pole ($\theta = 0$). $\theta\epsilon$ [0, 360] gives the counterclockwise angular deviation in the plane from the axis that points directly toward the monkey ($\phi = 0$). Thus a reaching direction in the horizontal plane starting at the center position and moving directly toward the monkey's body is given by the (θ, ϕ) pair (90°, 0°), whereas a reach directly away from the body is given by (90°, 180°).

MODELS OF PD DISTRIBUTIONS. The parametric density estimation procedures described in the companion paper was used to estimate PD distributions contained within local regions of the map of recording sites.

MODEL SELECTION. Local distributions of PDs were classified as uniform, unimodal, or bimodal by applying successively appropriate statistical tests. First, we determined whether the hypothesis of a uniform distribution could be rejected in favor of a unimodal (Rayleigh test, $P < 0.05$) or bimodal (Bingham test, $P < 0.05$) alternative. A distribution for which uniformity could be rejected by either of these tests was considered nonuniform; otherwise, the distribution was labeled uniform (for lack of a more appropriate model). A distribution for which uniformity was rejected only by the Rayleigh test was

considered unimodal. A distribution for which uniformity was rejected only by the Bingham test was considered bimodal. In cases where uniformity was rejected by both tests, we used a likelihood-ratio bootstrapping procedure (McLachlan and Peel 2000) to test for bimodality against the null hypothesis of a unimodal distribution. In this procedure, distributions were fit with both unimodal and bimodal mixture models (Banerjee et al. 2003; see companion paper for details of fitting procedure) and L_1 and L_2, the likelihood of the data under the unimodal and bimodal models, respectively, were used to construct a log-likelihood ratio for the data: $L = -\log(L_1/L_2)$. Then, 1,000 random sets of PDs were generated from the distribution defined by the parameters of the unimodal fit to the original data. These generated sets were separately fit by a unimodal and a bimodal mixture model and the log-likelihood ratio under these models (L') was determined. If L was found to be significantly ($P < 0.05$) larger than L', the distribution was considered bimodal; otherwise, it was considered unimodal. The procedure is described in detail in McLachlan and Peel (2000).

Population vector

Let $r_i(\mathbf{d})$ be the average of all firing rates observed for cell i while the monkey performed a reach in direction $\mathbf{d}$. The neuronal population vector (NPV) for this direction was calculated as $NPV(\mathbf{d}) = \sum \mathrm{r_i}(\mathbf{d}) \cdot \mathbf{p}_i$, using the normalized firing rates, $\mathrm{r_i}(\mathbf{d}) = [r_i(\mathbf{d}) - b_i]/k_i$, where $\mathbf{p}_i$ is the preferred direction of cell i, and b_i and k_i are the baseline and gain terms defined in the companion paper. The error of the NPV is expressed as the angle between $NPV(\mathbf{d})$ and $\mathbf{d}$.

RESULTS

The distribution of preferred directions

We analyzed PDs extracted from MUA at 981 recording sites distributed across the surface of the primary motor cortex in two monkeys (monkey A: 495 sites, monkey B: 486 sites). We refer to the collection of PDs from all sites for a single monkey as the *global population* and refer to its distribution as the *global distribution* (this is to be contrasted against *local* populations and *local* distributions). In the companion paper, it was shown that the distribution of PDs extracted from the SUA of a subset of the sites considered here displayed a characteristic structure. Here, we repeated our analysis of the PD distribution for PDs extracted at the larger number of sites for which MUA was available.

An equal-area projection plot of each PD and a nonparametric estimate of the global distribution for both monkeys are shown in Fig. 1. These plots bear out the salient aspects of the global distribution of PDs revealed in the companion paper and demonstrate that the main results hold regardless of whether PDs are extracted from single- or multiunit activity.

As in the companion paper, we quantified the characteristics of the global PD distribution using a two-component mixture model (Banerjee et al. 2003)

$$g(\mathbf{x}) = \sum_{i=1}^{2} \alpha_i f(\mathbf{x}|\kappa_i, \mu_i)$$

In this model, $g(\mathbf{x})$ gives the density of PDs in the neighborhood of the reaching direction $\mathbf{x}$. The components of the model are weighted von Mises–Fisher distribution functions, where $i = 1$ denotes the forward component and $i = 2$ denotes the backward component. We refer to the μ parameter of each component as its "primary direction" because it specifies the direction of reach about which the PDs in each component are

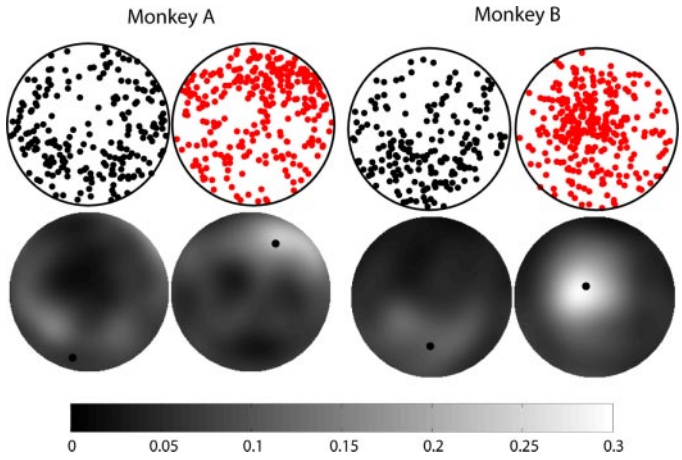

FIG. 1. Global distribution of preferred directions (PDs). *Top row*: equal area projection plot of PDs. For each monkey, the circle on the *left* corresponds to reaches made from the center position toward the body; circle on the *right* corresponds to reaches away from the body. *Bottom row*: equal area projection plots of the nonparametric estimate of PD density. Grayscale indicates the density of PDs at each node of a finely spaced grid covering the surface of the sphere. Black dots indicate the global primary directions identified by the 2-component mixture model.

clustered. The polar components of a primary direction are denoted $\mu(\theta)$ and $\mu(\phi)$; the angle between the forward and backward primary directions is given by $\omega \equiv acos\ (\boldsymbol{\mu}_1 \cdot \boldsymbol{\mu}_2)$. κ is a concentration parameter that determines the intensity of clustering within each component. α is the component weight and may be interpreted as the prior probability that a randomly selected PD will belong to a given component. Fitted values of the model parameters are given in Table 1.

The nonuniform structure of the PD distribution leads naturally to questions about the spatial distribution of PDs. Given what is known about somatotopic organization in M1, it is possible that two peaks in the global distribution are generated by PDs that are clustered together in distinct, spatially separated cortical regions. Another possibility is that the features of the global distribution are replicated locally, so that the distribution of PDs in any local region of M1 may have the same properties as the distribution of PDs taken from across all regions of M1. To test between these possibilities, we examined the surface map of PDs. We first determined a functionally meaningful size for a "local region" of cortex. We then analyzed the distribution of PDs within these local regions by applying the mixture model separately to PDs taken from such regions situated at points on a regular grid covering the cortical surface. Mixture models of order >2 were not considered because the global distribution shows strong evidence for only two components.

Before presenting an analysis of the map of PDs, it is important to note that the recording sites in our sample were spread across all cortical layers. To determine whether different cortical layers exhibited appreciable differences in the structure of their PD distributions, we separated recording sites into subpopulations according to whether they occupied the superficial (layers 2 and 3), middle (layer 5), or deep (layer 6) layers of the cortex. The PD distributions for these layer-specific subpopulations were then analyzed separately. We found that the basic structure of the global distribution, described above, remained unchanged across layers. Therefore

TABLE 1. *Parameters of the mixture model of the global distribution of each monkey*

		Forward Component			Backward Component			
Monkey	Number of MUA Sites	α_1	κ_1	μ_1,deg (θ,ϕ)	α_1	κ_1	μ_2,deg (θ,ϕ)	ω
A	495	0.47	3.33	(41.2, 143.9)	0.53	0.9	(157.5, 319.5)	161.1
B	486	0.42	5.14	(79.3, 189.3)	0.58	1.02	(143.0, 358.7)	136.8

the cortical layer(s) occupied by sites from a particular local region was not considered in subsequent analyses.

A surface map of preferred directions in M1

Surface maps of PDs are shown in Figs. 2 and 3. To construct these maps, the position of each recording site containing a significant PD was projected to the cortical surface along its local anatomical column. The cortical surface was then unfolded about the central sulcus (Naselaris et al. 2005). In these unfolded surface maps, the left/right borders run parallel to the central sulcus, with the most medial position located at the top. The top/bottom borders are orthogonal to the central sulcus, with the fundus located on the far left, and the crown is located near the center of each map. We will refer to these as the *s*-axis (parallel to the sulcus) and *m*-axis (nearly parallel to the midline), respectively (the illustration at *bottom* of Fig. 2 shows the relation of the axes to the anterior/posterior and medial/lateral axes). The θ and ϕ components of the PDs are given by separate, registered maps.

An obvious feature of the maps is the re-representation of polar angles at locations across the full extent of the recorded

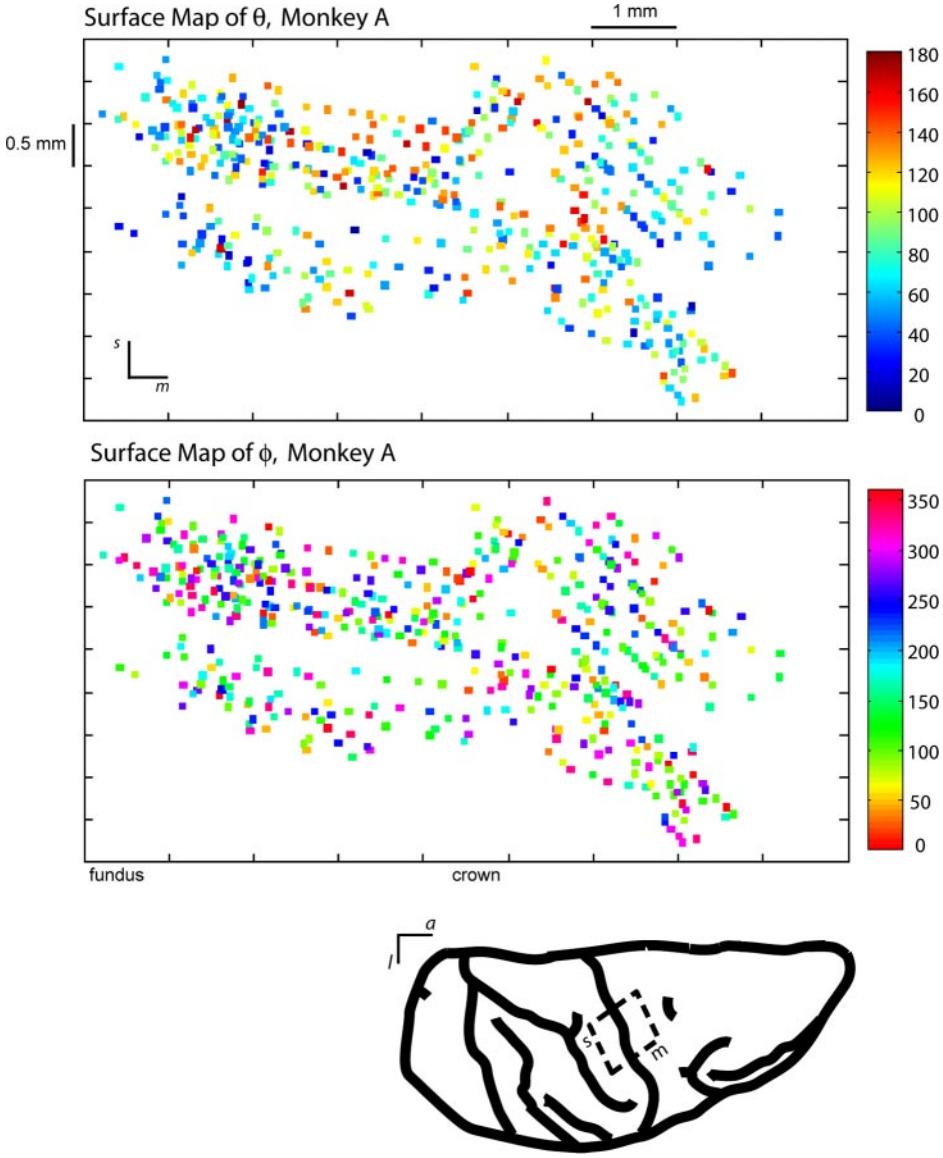

FIG. 2. Surface maps of the preferred directions, monkey A. Unfolded surface maps of PDs. Recording sites are marked by colored squares. θ component of each PD (*top row*) is coded on a linear color scale (blue = 0°, red = 180°); the ϕ component of each PD (*bottom row*) is coded on a circular color scale (red = 0°/360°). *Inset*: line drawing of the surface of the recorded hemisphere. Axes in the *top left* are anterior/posterior (*a*) and medial/lateral (*l*). Recording sites were confined to the area within the dashed parallelogram, the borders of which are aligned with the *s* and *m* axes.

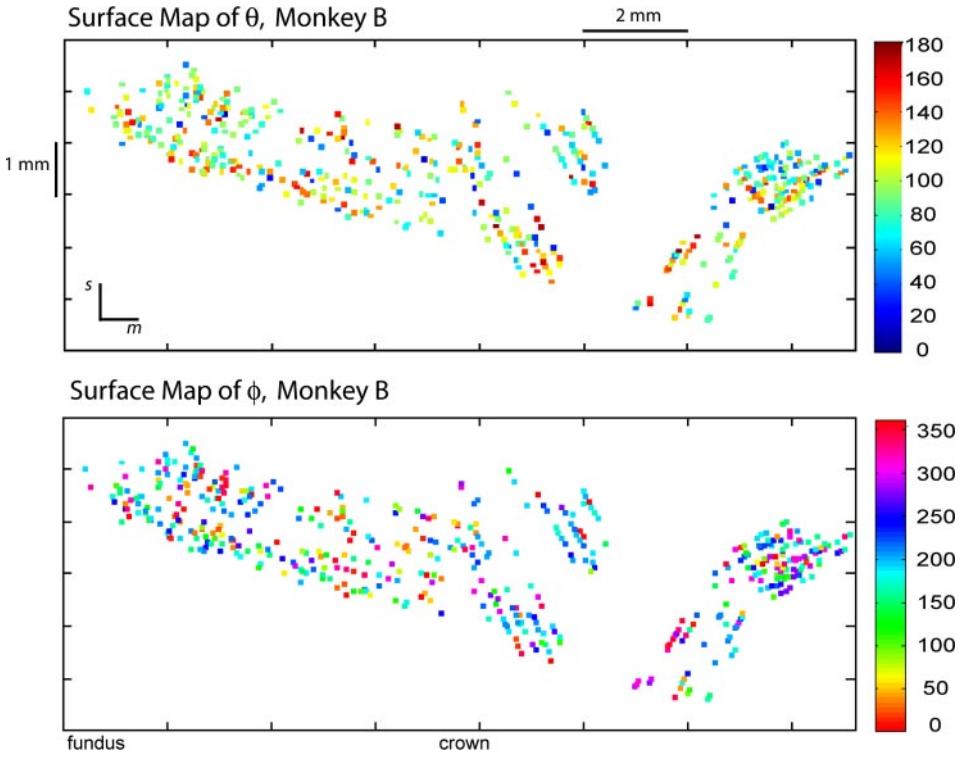

FIG. 3. Surface maps of the preferred directions, monkey B. Conventions are the same as for Fig. 2.

region, as well as the heterogeneous mix of angles within any localized subregion. Despite this widely distributed representation of polar angles, variation in the number of local PDs pointing in specific directions may also be appreciated. It is unclear from simply observing the surface map whether these variations reflect significant biases toward specific directions within localized cortical regions.

Another method for viewing the spatial pattern of PDs is to categorize each PD into one of eight octants that divide the sphere into equal areas and then plot the category membership of each PD at its respective site on the surface map. These maps are shown in Fig. 4. The impression given by these octant maps is consistent with the maps of the polar angular components: any given octant is represented at widely scattered points

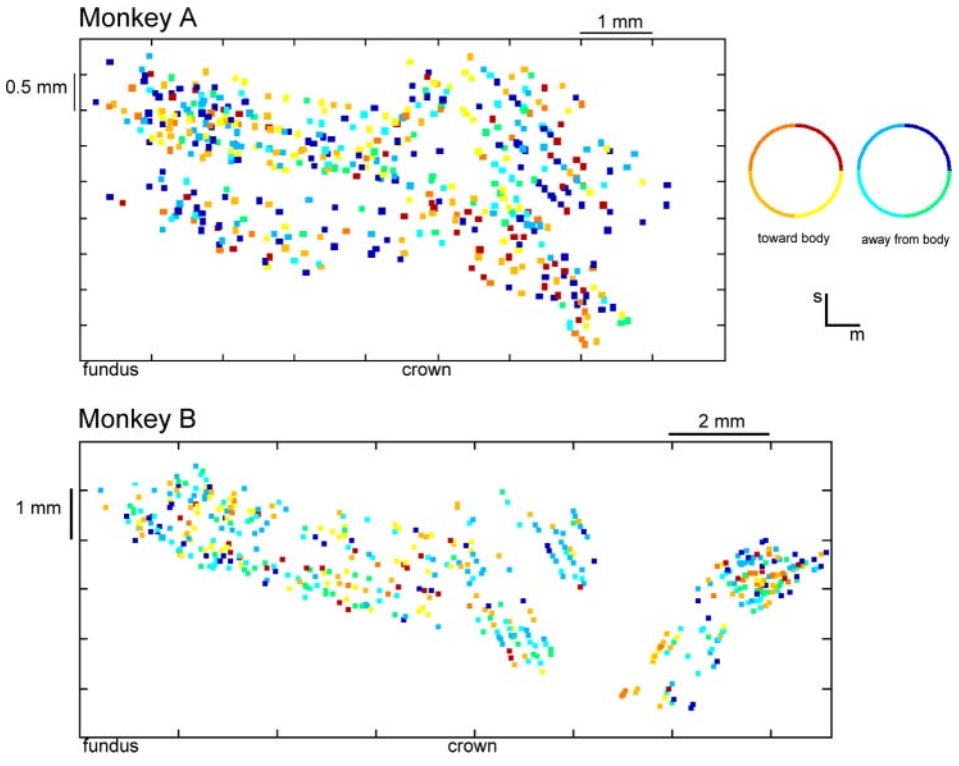

FIG. 4. Octant maps of preferred directions. Each PD is colored according to its membership in one of 8 octants that partition the surface of the sphere into equal areas. Colored rings indicate the position of each octant on the surface of the sphere; perspective is that of the monkey looking at the targets.

on the map and any given local region of the map contains multiple octants.

The spatial scale of PD dispersion

The PD maps presented above indicate that the distribution of PDs within local regions of the map may be dispersed across the full directional continuum. We estimated the size of the local region in which the full complement of PDs is represented by counting the number of empty octants within a radially expanding circular border centered on each recording site on the map. The result of this analysis (Fig. 5) indicates that the median radius of the cortical patch containing all octants is about 1 mm. It is important to note that because we could not sample all cells within regions of this size (in our experiments, the average number of samples for such regions was about 40), this figure represents an upper bound on the size of the region required to fill all octants. Thus we can assert that PD distributions in local regions with radius at most 1 mm replicate the structure of the global distribution in their covering of the sphere. In what follows, we will use the term "local region" to refer to any contiguous patch of cortex with a surface area of $\pi \approx 3$ mm^2.

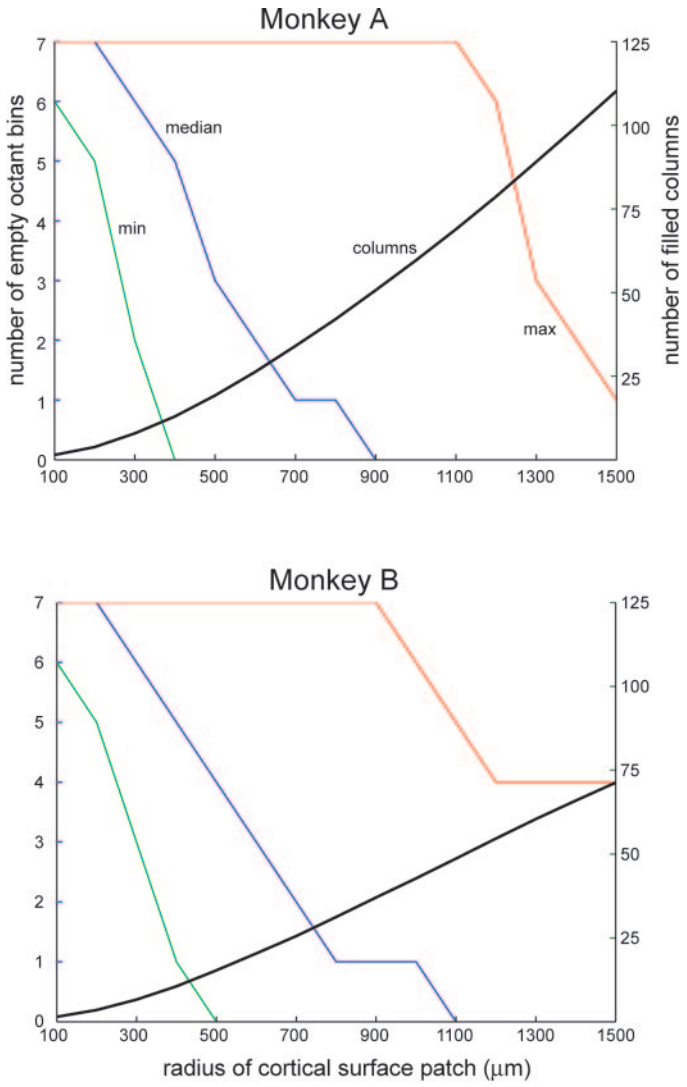

FIG. 5. Spatial scale of PD dispersion. Number of empty octants was counted for the set of PDs within a circular region of a given radius (abscissa) centered at each recording site. Minimum, median, and maximum number of empty octants (*left axis*) as a function of radius is shown by the green, blue, and red lines, respectively. Black line shows the average number of column-sized (80-μm diameter) patches within each circular region that contained a recording site (*right axis*).

To estimate the number of cortical columns that would be required to fill all eight PD octants, we also counted the number, within each circular region, of cortical-column–sized (80-μm diameter) patches that contained a recording site. This count revealed that the median number of cortical columns required to fill out all eight octants is at most 50 (Fig. 5).

Assessment of the nonuniformity of local distributions

Having determined the size of the local region required to cover all octants of the sphere, we analyzed local distributions from across the recorded area to determine whether the enrichment of forward and backward reaching directions that is seen globally is also present locally. We examined distributions of PD populations within square-shaped, overlapping local regions with a side of 1.6 mm, spaced at 400-μm intervals (surface area $\cong$ 2.5 mm^2). Statistical tests were applied in series to classify each local distribution as uniform, unimodal, or bimodal. Figure 6 shows the map of local distribution types. The maps demonstrate a preponderance of nonuniform local distributions (monkey A: 70%, $n = 87$; monkey B: 86%, $n = 163$), with the majority of local regions being bimodal (monkey A: 53%, $n = 66$; monkey B: 53%, $n = 100$).

Comparison of local to global primary directions

The primary direction(s) estimated in each nonuniform local region are shown under an equal-area projection in Fig. 7. It is evident from this figure that the local primary directions cluster in the forward and backward directions, similar to the global primary directions. The histogram of ω values for bimodal local regions underscores this similarity; each histogram shows a distinct peak near the ω for the corresponding global distribution (see Table 1). The local median ω for monkey A is 157°; for monkey B, the local median ω is 141°.

Figure 7 demonstrates the variation of the local primary directions about their global counterparts. We denote the angle between a local primary direction and its global counterpart as ξ_i, where $i = 1$ refers to the forward direction and $i = 2$ to the backward direction. Averaging across bimodal regions in both monkeys, the mean ± SD for ξ_1 is 25 ± 15°; for ξ_2 it is 43 ± 23 ° ($n = 164$). In both cases, this is significantly less than the 90 ° of angular deviation that would be expected from a uniform distribution of local primary directions (t-test, $P < 0.01$).

In most unimodal local regions (71%), the single-component model of the local distribution identifies a local primary direction (also shown in Fig. 7) that is closest to the forward global primary direction ($\xi_1 = 29 \pm 13°$, $n = 84$). Interestingly, the local primary directions obtained by fitting the two-component mixture model to local distributions classified as uniform also show significantly smaller deviation from the global primary directions than would be expected by chance ($P < 0.01$; ξ_1: 34.9 ± 23.4, ξ_2: 48.8 ± 22.9, $n = 59$). This implies that local regions defined as uniform also contain enhancements in the forward and backward directions that are too weak to be detected by a significance criterion of $P < 0.05$.

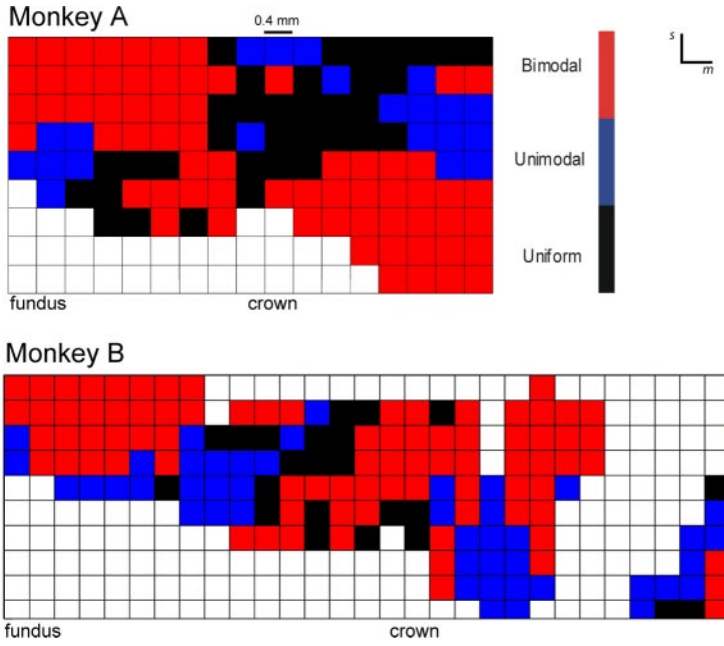

FIG. 6. Surface maps of distribution type. This map was constructed by partitioning the cortical surface into overlapping squares spaced at 400 μm with a side of 1.6 mm. Distribution of PDs in each region is classified as uniform (black), unimodal (blue), or bimodal (red).

Assessment of local concentration parameters and component weights

The median κ_1 component of the bimodal local distributions was significantly larger than the median κ_2 ($P < 0.01$, two-sample sign test), consistent with the relative sizes of these parameters in the global distribution. For Monkey A, the medians of κ_1 and κ_2 were 4.2 and 2.0, respectively. For Monkey B, medians were 6.5 and 2.6. The median sizes of the local κ values are larger than their global counterparts (see Table 1); this result is most easily explained by the variation in local primary directions, which will have the effect of "spreading out" the global distribution.

The distribution of local α values was consistent with the nearly equal weights estimated for the forward and backward components of the global distribution (see Table 1). For monkey A, the median $\alpha_1 = 0.49$; for monkey B, the median was 0.57.

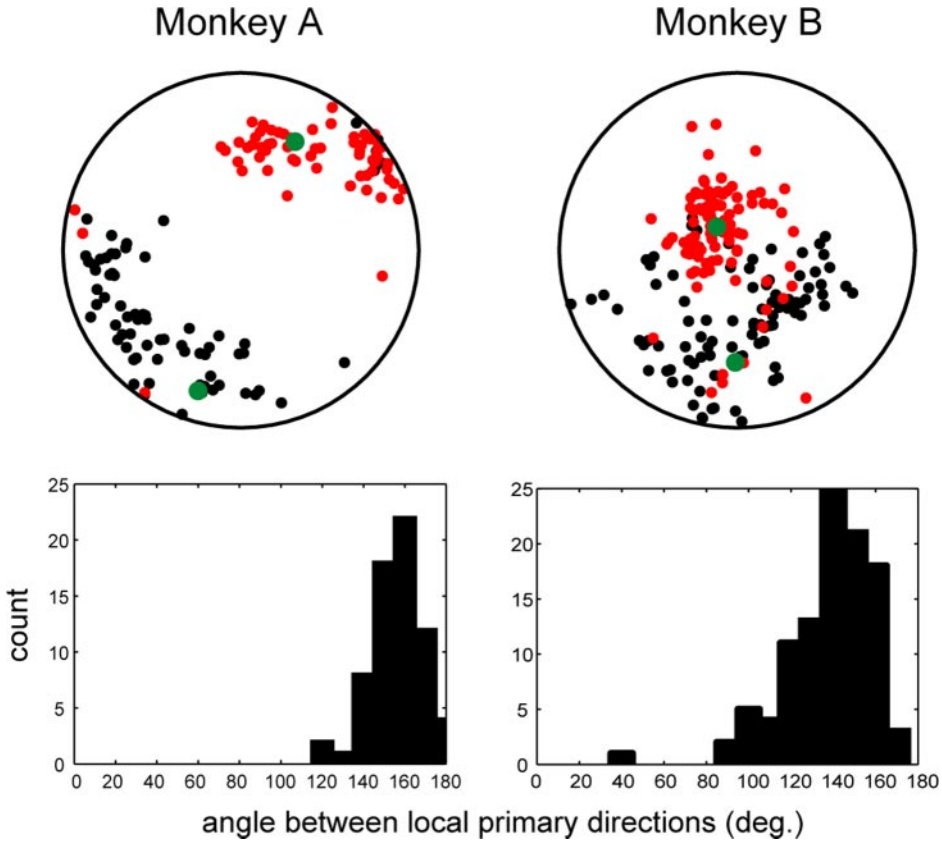

FIG. 7. Distribution of local primary directions. *A*: a mixture model was fit to the distribution of PDs in each local region defined as nonuniform. Primary direction(s) from each of these local regions is shown under an equal area projection, where red dots indicate the forward hemisphere and black dots the backward hemisphere. Primary directions for the global distribution are shown as large green dots. *B*: histogram of ω, the angle between the forward and backward primary direction in each bimodal local region.

Spatial variation in decoding accuracy

We have demonstrated that, on average, all octants of the sphere are represented by the distribution of PDs within a local region. This finding implies that a reasonably accurate estimate of reaching direction should be obtainable from the population activity generated by cells contained within a local region. To test this hypothesis, we calculated the error of the neuronal population vector (NPV) applied to the population activity of cells within a radially expanding circular border centered on each recording site. Figure 8 demonstrates that the average NPV error for local populations (cells contained within a circular surface patch of radius 0.8–1 mm) comes within roughly one SD of the error sustained by the global population (dashed lines in Fig. 8). It is again important to note that these calculations represent an upper bound on the error; a more dense sampling of activity within the local regions would most likely reveal a much sharper decrease in NPV error as a function of the local region size.

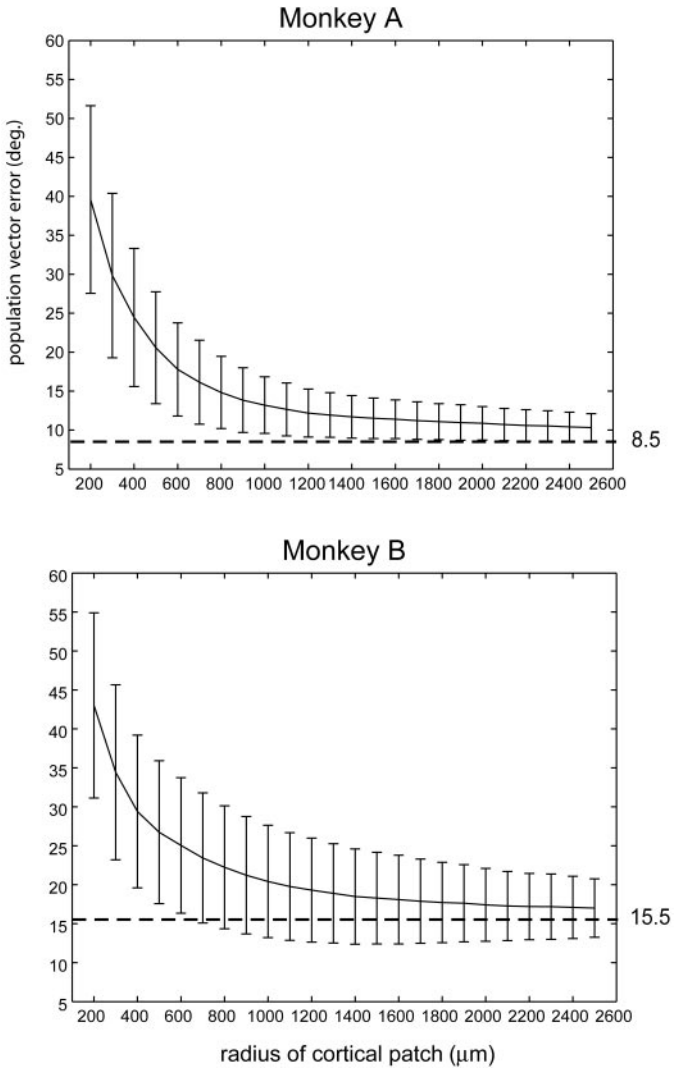

FIG. 8. Spatial scaling of population vector error. A population vector estimate of reaching direction was derived from activity at all sites within a given radius (abscissa) of each recording site on the surface map. For a fixed radius, population vector error was averaged across all reaching directions and all sites (ordinate axis; error bars give SD across sites). Dashed line indicates the global error obtained by using activity from all recording sites.

To determine whether the variation in NPV error across local regions was spatially mapped, we calculated the NPV for local populations within the same set of overlapping square patches used above. Because NPV error decreases with the number of cells used to construct the NPV, we applied a bootstrapping procedure to control for correlated fluctuations in the number of recording sites. We constructed 10^3 "shuffled" PD maps. In the shuffled maps, PDs from the original map were randomly assigned to a different recording site. For each of the shuffled maps, NPV error was measured in each local region. The distribution of NPV errors, in each local region of the shuffled maps, was then compared with the error obtained from the corresponding local region in the original PD map. Figure 9 displays the surface area covered by the local regions in which NPV error was significantly less than (blue areas) or greater than (red areas) the NPV errors obtained at the same location in the shuffled maps ($P < 0.05$). Consistent across both monkeys is an area near the crown in which NPV error is significantly suppressed and an area covering the fundus in which NPV error is significantly inflated. For monkey A, the average error in the suppressed local regions is $8.3 \pm 1.2°$; in the inflated regions it is $22.7 \pm 6.8°$. For monkey B, the errors are 14.2 ± 8.4 and $37.1 \pm 10.8°$, respectively.

Because the significant variations in NPV error are independent of sample size, they may be related to differences in the amount of dispersion in the local PD distributions. This assumption is consistent with the fact that both monkeys exhibit overlapping uniform regions near the crown and overlapping nonuniform regions near the fundus (Fig. 5). To test the assumption explicitly, we compared the NPV error to a measure of the local clustering of PDs: $\sigma \equiv \alpha_1\kappa_1 + \alpha_2\kappa_2$. This intuitive measure of clustering will increase as κ increases and weights the amount of clustering in each component of the model by its overall contribution to the distribution (α). Figure 10 shows that much of the variation in NPV error can be explained by variation in the clustering of the underlying population of PDs ($r = 0.69$; $P < 0.01$).

DISCUSSION

We have analyzed the large-scale spatial organization of M1 in the context of its representation of reaching direction. We obtained PDs from multiple recording sites across a large extent of the arm representation in M1 and projected each site along its anatomical column, resulting in a two-dimensional map of PDs along the cortical surface. Our analysis of this map revealed the following fundamental properties of the motor-cortical representation of reaching direction: *1*) any given reaching direction is represented at multiple sites from across the full extent of the arm region of M1; *2*) the majority of localized, contiguous cortical regions with surface area of at most about 3 mm^2 contain a representation of the full 3D continuum of reaching directions; *3*) the distribution of PDs within most regions of this size contain an enrichment of the representation for the same forward and backward "primary" directions; and *4*) variations in the breadth or dispersion of local PD distributions account for systematic differences in the decoding error associated with particular local regions; this error is lowest for regions near the crown and highest for regions in the fundus of the central sulcus.

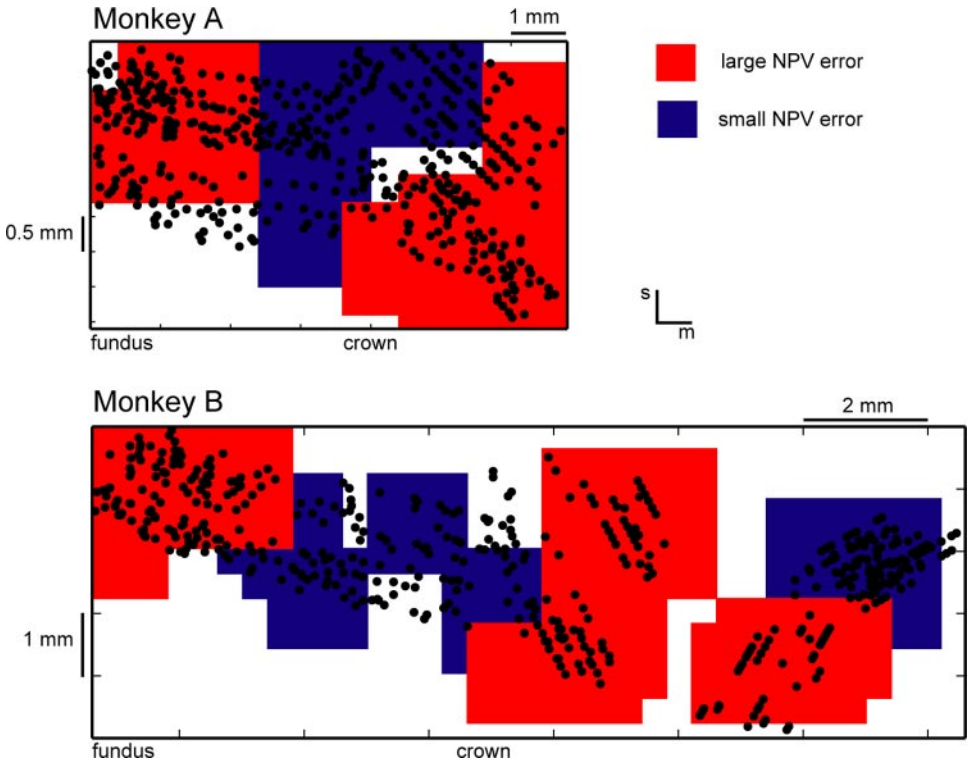

FIG. 9. Regions of large and small neuronal population vector (NPV) error. Blue and red regions superimposed on the surface map of recording sites (black dots) indicate regions of significantly small (blue) or large (red) NPV error, as determined by a bootstrapping procedure.

Previous studies focused on short-range structure, comparing the differences in PDs at sites separated by small (<500-μm) distances. The main results of these studies were the following: *1*) cells within vertical columns of diameter around 80 μm contain a representation of similar (<45° of angular deviation) reaching directions (Amirikian and Georgopoulos 2003; Georgopoulos et al. 1984); *2*) cells displaced along the tangential dimension by <150 μm are highly likely (significantly more likely than random) to represent similar reaching directions (Amirikian and Georgopoulos 2003; Ben-Shaul et al. 2003); and *3*) cells displaced at larger (≈400-μm) distances are highly likely to represent divergent reaching directions (>120° of angular deviation) (Amirikian and Georgopoulos 2003).

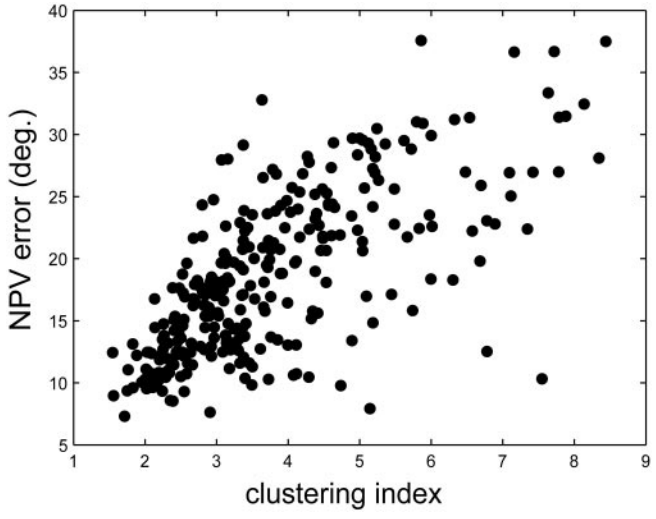

FIG. 10. NPV error is plotted against a measure of PD clustering, constructed from the component weights and concentration parameters of the mixture model fits to each local distribution.

This list of recent findings refines our picture of the neural representation of 3D reaching in the motor cortex. The motor cortex may be considered as an assemblage of overlapping regions with a surface area of about 3 mm^2. Within these regions, the diversity of cells' PDs is sufficient to represent any given direction of reach. In many such regions, we find an enrichment for forward and backward reaching. The spatial organization of PDs within these regions is nonrandom: PDs are organized into columns and they are correlated across very small distances along the tangential dimension, beyond which their arrangement appears to have a periodic structure.

In the next subsections, we will attempt to relate these features of directional organization to known facts regarding motor-cortical projections to motoneuronal pools and use-dependent plasticity in the motor cortex.

Somatotopic organization and the organization of preferred directions

Work on primary motor cortex in the past several decades reflects a growing appreciation of the distributed nature of somatotopic representation in this area (Asanuma and Rosen 1972; Donoghue et al. 1992; Gould et al. 1986; Kwan et al. 1978; Sanes and Schieber 2001; Schieber 2001; Schieber and Hibbard 1993). Assessment of the anatomical convergence (Andersen et al. 1975; Darian-Smith et al. 1990; Jankowska et al. 1975) and divergence (Shinoda et al. 1981) of cortico-spinal inputs and the application of sensitive tools (such as stimulus-triggered and spike-triggered averaging) for revealing connections between M1 neurons and muscle activity have helped to define two main aspects of distributed somatotopy: *1*) single cells in M1 make weighted contributions to multiple muscles,

typically three (Cheney et al. 1985; Donoghue et al. 1992; McKiernan et al. 1998; Park et al. 2001; Shinoda et al. 1981), and *2*) a single muscle is represented in repeated fashion at multiple locations across M1 (Asanuma and Rosen 1972; Donoghue et al. 1992; Gould et al. 1986; Kwan et al. 1978).

How are these aspects of M1's somatotopic organization linked to its representation of reaching direction? We have shown that cortical patches with a median surface area of at most 3 mm^2 are sufficient to encompass the full range of reaching directions. Given the divergent nature of the somatotopic organization, the cells contained within a local region will have access to not one muscle but a group of muscles. Under such an arrangement, each cell could make a contribution to an arm reach in the direction of its own PD by making a differentially weighted contribution to the activation of the muscles accessible by the local region. The divergence of somatotopic representation thus provides an ideal substrate for translating the directional signal generated by a local region. This interpretation of motor-cortical organization was the basis of the original explanation for how directional signals generated by the cortex could be translated into a reaching movement (Georgopoulos 1988; Schwartz et al. 1988) and has received some measure of experimental (Lewis and Kristan 1998) and theoretical (Georgopoulos 1988, 1996) support.

Another fact about the somatotopic organization of M1 is characterized by the familiar motor homunculus. Large-scale gradients in the somatotopic organization can be uncovered if thresholding and classification methods are applied in constructing the motor map. A commonly used example of such a method is threshold-intracortical microstimulation (tICMS), which has been used to study somatotopic organization in anesthetized animals. In tICMS, sites on the map are stimulated at current amplitudes just large enough to evoke movement about a single joint (Asanuma and Rosen 1972; Kwan et al. 1978). The application of tICMS allows researchers to identify each stimulated site with a single joint or body part, in spite of the fact that many muscles, joints, and even complex movements are likely to be activated by larger stimulation amplitudes.

It may be tempting to draw an analogy between "primary" directions and "dominant" muscles detected by tICMS: the primary directions in a local region are those most likely to be represented, whereas the dominant muscles are those that are easiest to detect. This analogy fails in the face of our observation that the enrichment of the representation for forward and backward reaching directions occurs in local regions spread across the arm region in M1. Thus similar primary directions exist in local regions that are most likely "dominated" by different muscle representations.

Comparison with preferred orientation maps in primary visual cortex (V1)

There are two important similarities between the spatial organization of PDs in M1 and that of orientation preference in V1 (Hubel and Wiesel 1974, 1977). First, M1 exhibits short-range correlations between PDs (Amirikian and Georgopoulos 2003; Ben-Shaul et al. 2003). Such correlations are consistent with the smooth variation of orientation preference observed in V1. Second, we have shown here that the size of the cortical module containing the full complement of PDs is of the same order as the size of a hypercolumn in V1, which contains a full set of isoorientation lines. Some have attributed these features of visual cortical organization to the competing principles of continuity and coverage (Swindale et al. 2000); it is possible that these ideas could be generalized to account for spatial organization in the motor cortex as well.

In V1, preferred orientations within a hypercolumn display a pinwheel organization (Blasdel 1992; Bonhoeffer and Grinvald 1991). Orientation is a one-dimensional parameter, whereas PDs are two-dimensional; therefore pinwheel organization could not, even in principle, be replicated exactly in the motor cortex. Further analysis and experiments—such as the use of optical imaging in the motor cortex—will be required to determine whether there is anything similar to pinwheel organization in the motor cortex.

Plasticity in the motor cortex and the distribution of PDs

In the companion paper, we conjectured that the enrichment of the motor-cortical representation for forward and backward reaching directions may simply reflect an increase in the incidence of reaches in these directions, relative to other directions, in the everyday life of the monkey. Because the repetition of specific movements leads to an enlargement of the cortical territory devoted to representing that movement (Nudo et al. 1996), this conjecture predicts that the representation of the primary directions should be widespread. Our findings are certainly consistent with this prediction: forward and backward primary directions constitute a significant feature of local distributions scattered across the entirety of our recorded area. A direct test of this conjecture, however, would require a characterization of the statistics of the natural reaching behavior of the monkey and a thorough sampling of PDs taken before and after intentional manipulation of these statistics. To our knowledge, such an experiment has not yet been attempted.

Spatial distribution of decoding error

It would have been difficult to predict—from currently known facts about M1 structure—a local minimum in the NPV error near the crown. It would be worth exploring the relationship between NPV error and the pattern of motor-cortical outputs (Darian-Smith et al. 1990), such as those to area 5, which are known to derive primarily from the crown of the central gyrus (Caminiti et al. 1985). Regardless of the cause of this variation, the finding also has a potentially practical application. Neuroprosthetics systems currently under design use neural signals extracted from the motor cortex (Taylor et al. 2002). Our finding suggests that a desirable location for recording electrodes in these systems is near the crown of the central sulcus and that the surface area spanned by an array of these electrodes need be at most about 3 mm^2.

REFERENCES

Amirikian B and Georgopoulos AP. Modular organization of directionally tuned cells in the motor cortex: is there a short-range order? *Proc Natl Acad Sci USA* 100: 12474–12479, 2003.

Andersen P, Hagan PJ, Phillips CG, and Powell TP. Mapping by microstimulation of overlapping projections from area 4 to motor units of the baboon's hand. *Proc R Soc Lond B Biol Sci* 188: 31–36, 1975.

Asanuma H and Rosen I. Topographical organization of cortical efferent zones projecting to distal forelimb muscles in the monkey. *Exp Brain Res* 14: 243–256, 1972.

Banerjee A, Inderjit D, Joydeep G, and Suvrit S. Generative model-based clustering of directional data. In: *Proceedings of the Ninth ACM SIGKDD International Conference on Knowledge Discovery and Data Mining*. Washington, DC: ACM Press, 2003, p. 19–28.

Ben-Shaul Y, Stark E, Asher I, Drori R, Nadasdy Z, and Abeles M. Dynamical organization of directional tuning in the primate premotor and primary motor cortex. *J Neurophysiol* 89: 1136–1142, 2003.

Blasdel GG. Orientation selectivity, preference, and continuity in monkey striate cortex. *J Neurosci* 12: 3139–3161, 1992.

Bonhoeffer T and Grinvald A. Iso-orientation domains in cat visual cortex are arranged in pinwheel-like patterns. *Nature* 353: 429–431, 1991.

Caminiti R, Johnson PB, Galli C, Ferraina S, and Burnod Y. Making arm movements within different parts of space: the premotor and motor cortical representation of a coordinate system for reaching to visual targets. *J Neurosci* 11: 1182–1197, 1991.

Caminiti R, Zeger S, Johnson PB, Urbano A, and Georgopoulos AP. Corticocortical efferent systems in the monkey: a quantitative spatial analysis of the tangential distribution of cells of origin. *J Comp Neurol* 241: 405–419, 1985.

Cheney PD and Fetz EE. Comparable patterns of muscle facilitation evoked by individual corticomotoneuronal (CM) cells and by single intracortical microstimuli in primates: evidence for functional groups of CM cells. *J Neurophysiol* 53: 786–804, 1985.

Cheney PD, Fetz EE, and Palmer SS. Patterns of facilitation and suppression of antagonist forelimb muscles from motor cortex sites in the awake monkey. *J Neurophysiol* 53: 805–820, 1985.

Darian-Smith C, Darian-Smith I, and Cheema SS. Thalamic projections to sensorimotor cortex in the macaque monkey: use of multiple retrograde fluorescent tracers. *J Comp Neurol* 299: 17–46, 1990.

Donoghue JP, Leibovic S, and Sanes JN. Organization of the forelimb area in squirrel monkey motor cortex: representation of digit, wrist, and elbow muscles. *Exp Brain Res* 89: 1–19, 1992.

Fetz EE and Cheney PD. Muscle fields of primate corticomotoneuronal cells. *J Physiol (Paris)* 74: 239–245, 1978.

Fetz EE and Cheney PD. Postspike facilitation of forelimb muscle activity by primate corticomotoneuronal cells. *J Neurophysiol* 44: 751–772, 1980.

Fischl B, Sereno MI, Tootell RB, and Dale AM. High-resolution intersubject averaging and a coordinate system for the cortical surface. *Hum Brain Mapp* 8: 272–284, 1999.

Georgopoulos AP. Neural integration of movement: role of motor cortex in reaching. *FASEB J* 2: 2849–2857, 1988.

Georgopoulos AP. On the translation of directional motor cortical commands to activation of muscles via spinal interneuronal systems. *Brain Res Cogn Brain Res* 3: 151–155, 1996.

Georgopoulos AP, Kalaska JF, Caminiti R, and Massey JT. On the relations between the direction of two-dimensional arm movements and cell discharge in primate motor cortex. *J Neurosci* 2: 1527–1537, 1982.

Georgopoulos AP, Kalaska JF, Crutcher R, Caminiti R, and Massey JT. The representation of movement direction the motor cortex: single cell and population studies. In: *Dynamic Aspects of Neocortical Functions*, edited by Edelman GM. New York: Wiley, 1984.

Georgopoulos AP, Schwartz AB, and Kettner RE. Neuronal population coding of movement direction. *Science* 233: 1416–1419, 1986.

Gould HJ 3rd, Cusick CG, Pons TP, and Kaas JH. The relationship of corpus callosum connections to electrical stimulation maps of motor, supplementary motor, and the frontal eye fields in owl monkeys. *J Comp Neurol* 247: 297–325, 1986.

Hubel DH and Wiesel TN. Sequence regularity and geometry of orientation columns in the monkey striate cortex. *J Comp Neurol* 158: 267–293, 1974.

Hubel DH and Wiesel TN. Ferrier lecture. Functional architecture of macaque monkey visual cortex. *Proc R Soc Lond B Biol Sci* 198: 1–59, 1977.

Humphrey DR and Reed DJ. Separate cortical systems for control of joint movement and joint stiffness: reciprocal activation and coactivation of antagonist muscles. *Adv Neurol* 39: 347–372, 1983.

Huntley GW and Jones EG. Relationship of intrinsic connections to forelimb movement representations in monkey motor cortex: a correlative anatomic and physiological study. *J Neurophysiol* 66: 390–413, 1991.

Jankowska E, Padel Y, and Tanaka R. Projections of pyramidal tract cells to alpha-motoneurones innervating hind-limb muscles in the monkey. *J Physiol* 249: 637–667, 1975.

Kwan HC, MacKay WA, Murphy JT, and Wong YC. Spatial organization of precentral cortex in awake primates. II. Motor outputs. *J Neurophysiol* 41: 1120–1131, 1978.

Lewis JE and Kristan WB Jr. A neuronal network for computing population vectors in the leech. *Nature* 391: 76–79, 1998.

Lurito JT, Georgakopoulos T, and Georgopoulos AP. Cognitive spatial-motor processes. 7. The making of movements at an angle from a stimulus direction: studies of motor cortical activity at the single cell and population levels. *Exp Brain Res* 87: 562–580, 1991.

McKiernan BJ, Marcario JK, Karrer JH, and Cheney PD. Corticomotoneuronal postspike effects in shoulder, elbow, wrist, digit, and intrinsic hand muscles during a reach and prehension task. *J Neurophysiol* 80: 1961–1980, 1998.

McLachlan G and Peel D. *Finite Mixture Models.* New York: Wiley, 2000.

Naselaris T, Merchant H, Amirikian B, and Georgopoulos AP. Spatial reconstruction of trajectories of an array of recording microelectrodes. *J Neurophysiol* 93: 2318–2330, 2005.

Nudo RJ, Milliken GW, Jenkins WM, and Merzenich MM. Use-dependent alterations of movement representations in primary motor cortex of adult squirrel monkeys. *J Neurosci* 16: 785–807, 1996.

Park MC, Belhaj-Saif A, Gordon M, and Cheney PD. Consistent features in the forelimb representation of primary motor cortex in rhesus macaques. *J Neurosci* 21: 2784–2792, 2001.

Penfield W and Boldrey E. Somatic motor and sensory representation in the cerebral cortex of man as studied by electrical stimulation. *Brain* 37: 389–443, 1937.

Penfield W and Rasmussen T. *The Cerebral Cortex of Man.* New York: Macmillan, 1950.

Sanes JN and Schieber MH. Orderly somatotopy in primary motor cortex: does it exist? *Neuroimage* 13: 968–974, 2001.

Schieber MH. Constraints on somatotopic organization in the primary motor cortex. *J Neurophysiol* 86: 2125–2143, 2001.

Schieber MH and Hibbard LS. How somatotopic is the motor cortex hand area? *Science* 261: 489–492, 1993.

Schwartz AB. Direct cortical representation of drawing. *Science* 265: 540–542, 1994.

Schwartz AB, Kettner RE, and Georgopoulos AP. Primate motor cortex and free arm movements to visual targets in three-dimensional space. I. Relations between single cell discharge and direction of movement. *J Neurosci* 8: 2913–2927, 1988.

Shinoda Y, Yokota J, and Futami T. Divergent projection of individual corticospinal axons to motoneurons of multiple muscles in the monkey. *Neurosci Lett* 23: 7–12, 1981.

Strick PL and Preston JB. Multiple representation in the primate motor cortex. *Brain Res* 154: 366–370, 1978.

Swindale NV, Shoham D, Grinvald A, Bonhoeffer T, and Hubener M. Visual cortex maps are optimized for uniform coverage. *Nat Neurosci* 3: 822–826, 2000.

Taylor DM, Tillery SI, and Schwartz AB. Direct cortical control of 3D neuroprosthetic devices. *Science* 296: 1829–1832, 2002.

Waters RS, Samulack DD, Dykes RW, and McKinley PA. Topographic organization of baboon primary motor cortex: face, hand, forelimb, and shoulder representation. *Somatosens Mot Res* 7: 485–514, 1990.